High-efficiency cascaded up and down conversion in nonlinear Kerr cavities

Chao Zhou and Peter Bermel*

Birck Nanotechnology Center and School of Electrical and Computer Engineering, Purdue University, West Lafayette, IN 47907, USA

**pbermel@purdue.edu*

Abstract: In this work, we derive general conditions to achieve high efficiency cascaded third harmonic generation and three photon parametric down conversion in Kerr nonlinear resonant cavities. We employ the general yet rapid temporal coupled-mode method, previously shown to accurately predict electromagnetic conversion processes in the time domain. In our study, we find that high-efficiency cascaded third harmonic generation can be achieved in a triply resonant cavity. In contrast, high-efficiency cascaded three-photon parametric down conversion cannot be achieved directly in a triply resonant cavity, although a combination of two doubly resonant cavities and three waveguides is an effective alternative. The stabilities of the calculated steady-state solutions for both processes are revealed by applying Jacobian matrices. Finally, we find that the inclusion of self- and cross- phase modulation introduces multi-stable solutions. Further study is required to find a simple way to reliably achieve stable conversion at the highest possible efficiency.

OCIS codes: (130.4310) Nonlinear; (190.3270) Kerr effect; (190.2620) Harmonic generation and mixing; (190.4410) Nonlinear optics, parametric processes; and (140.4780) Optical resonators.

References and links

1. P. A. Franken, A. E. Hill, C. W. Peters, and G. Weinreich, "Generation of optical harmonics," Phys. Rev. Lett. **7**, 118–119 (1961).
2. R. W. Boyd, *Nonlinear optics* (Academic press, 2003).
3. M. Soljačić and J. D. Joannopoulos, "Enhancement of nonlinear effects using photonic crystals," Nat. Mater. **3**, 211–219 (2004).
4. P. Bermel, A. Rodriguez, J. D. Joannopoulos, and M. Soljačić, "Tailoring optical nonlinearities via the purcell effect," Phys. Rev. Lett. **99**, 053601 (2007).
5. A. Rodriguez, M. Soljacic, J. D. Joannopoulos, and S. G. Johnson, "$\chi^{(2)}$ and $\chi^{(3)}$ harmonic generation at a critical power in inhomogeneous doubly resonant cavities," Opt. Express **15**, 7303–7318 (2007).
6. H. Hashemi, A. W. Rodriguez, J. Joannopoulos, M. Soljačić, and S. G. Johnson, "Nonlinear harmonic generation and devices in doubly resonant kerr cavities," Phys. Rev. A **79**, 013812 (2009).
7. M. C. Teich and B. Saleh, "Fundamentals of photonics," Wiley Interscience, Canada p. 3 (1991).
8. J. U. Fürst, D. V. Strekalov, D. Elser, M. Lassen, U. L. Andersen, C. Marquardt, and G. Leuchs, "Naturally phase-matched second-harmonic generation in a whispering-gallery-mode resonator," Phys. Rev. Lett. **104**, 153901 (2010).
9. M. Bieler, "Thz generation from resonant excitation of semiconductor nanostructures: Investigation of second-order nonlinear optical effects," IEEE J. Sel. Topics Quantum Electron. **14**, 458–469 (2008).
10. I. B. Burgess, Y. Zhang, M. W. McCutcheon, A. W. Rodriguez, J. Bravo-Abad, S. G. Johnson, and M. Lončar, "Design of an efficient terahertz sourceusing triply resonant nonlinearphotonic crystal cavities," Opt. Express **17**, 20099–20108 (2009).

11. J. Bravo-Abad, A. W. Rodriguez, J. D. Joannopoulos, P. T. Rakich, S. G. Johnson, and M. Soljačić, "Efficient low-power terahertz generation via on-chip triply-resonant nonlinear frequency mixing," Appl. Phys. Lett. **96**, 101110 (2010).
12. J. Hald, "Second harmonic generation in an external ring cavity with a brewster-cut nonlinear crystal: theoretical considerations," Opt. Commun **197**, 169 – 173 (2001).
13. R. Lifshitz, A. Arie, and A. Bahabad, "Photonic quasicrystals for nonlinear optical frequency conversion," Phys. Rev. Lett. **95**, 133901 (2005).
14. B. Freedman, G. Bartal, M. Segev, R. Lifshitz, D. N. Christodoulides, and J. W. Fleischer, "Wave and defect dynamics in nonlinear photonic quasicrystals," Nature **440**, 1166–1169 (2006).
15. Y. Morozov, I. Nefedov, V. Aleshkin, and I. Krasnikova, "Terahertz oscillator based on nonlinear frequency conversion in a double vertical cavity," Semiconductors **39**, 113–118 (2005).
16. T. J. Kippenberg, S. M. Spillane, and K. J. Vahala, "Kerr-nonlinearity optical parametric oscillation in an ultrahigh-q toroid microcavity," Phys. Rev. Lett. **93**, 083904 (2004).
17. M. M. Fejer, "Nonlinear optical frequency conversion," Phys Today **47**, 25–33 (1994).
18. V. S. Ilchenko, A. A. Savchenkov, A. B. Matsko, and L. Maleki, "Nonlinear optics and crystalline whispering gallery mode cavities," Phys. Rev. Lett. **92**, 043903 (2004).
19. F. S. Felber and J. H. Marburger, "Theory of nonresonant multistable optical devices," Appl. Phys. Lett. **28** (1976).
20. A. Parini, G. Bellanca, S. Trillo, M. Conforti, A. Locatelli, and C. D. Angelis, "Self-pulsing and bistability in nonlinear bragg gratings," J. Opt. Soc. Am. B **24**, 2229–2237 (2007).
21. A. R. Cowan and J. F. Young, "Optical bistability involving photonic crystal microcavities and fano line shapes," Phys. Rev. E **68**, 046606 (2003).
22. M. Soljačić, M. Ibanescu, S. G. Johnson, J. D. Joannopoulos, and Y. Fink, "Optical bistability in axially modulated omniguide fibers," Opt. Lett. **28**, 516–518 (2003).
23. M. F. Yanik, S. Fan, and M. Soljačić, "High-contrast all-optical bistable switching in photonic crystal microcavities," Appl. Phys. Lett. **83**, 2739–2741 (2003).
24. R. Smith, "Theory of intracavity optical second-harmonic generation," IEEE J. Sel. Topics Quantum Electron. **6**, 215–223 (1970).
25. L.-A. Wu, M. Xiao, and H. J. Kimble, "Squeezed states of light from an optical parametric oscillator," J. Opt. Soc. Am. B **4**, 1465–1475 (1987).
26. Z. Y. Ou and H. J. Kimble, "Enhanced conversion efficiency for harmonic generation with double resonance," Opt. Lett. **18**, 1053–1055 (1993).
27. V. Berger, "Second-harmonic generation in monolithic cavities," J. Opt. Soc. Am. B **14**, 1351–1360 (1997).
28. B. Maes, P. Bienstman, and R. Baets, "Modeling second-harmonic generation by use of mode expansion," J. Opt. Soc. Am. B **22**, 1378–1383 (2005).
29. M. Liscidini and L. Claudio Andreani, "Second-harmonic generation in doubly resonant microcavities with periodic dielectric mirrors," Phys. Rev. E **73**, 016613 (2006).
30. A. Ashkin, G. Boyd, and J. Dziedzic, "Resonant optical second harmonic generation and mixing," IEEE J. Sel. Topics Quantum Electron. **2**, 109–124 (1966).
31. K. Rivoire, Z. Lin, F. Hatami, and Vučković, "Sum-frequency generation in doubly resonant gap photonic crystal nanocavities," Appl. Phys. Lett **97**, 043103 (2010).
32. I. B. Burgess, A. W. Rodriguez, M. W. McCutcheon, J. Bravo-Abad, Y. Zhang, S. G. Johnson, and M. Lončar, "Difference-frequency generation with quantum-limited efficiency in triply-resonant nonlinear cavities," Opt. Express **17**, 9241–9251 (2009).
33. M. W. McCutcheon, D. E. Chang, Y. Zhang, M. D. Lukin, and M. Lončar, "Broad-band spectral control of single photon sources using a nonlinear photonic crystal cavity," arXiv:0903.4706 (2009).
34. Y. H. Avetisyan, "Cavity-enhanced terahertz region difference frequency generation in surface-emitting geometry," Proc. SPIE **3795**, 501–506 (1999).
35. R. A. Baumgartner and R. Byer, "Optical parametric amplification," IEEE J. Quant. Electron **15**, 432–444 (1979).
36. G. T. Moore, K. Koch, and E. Cheung, "Optical parametric oscillation with intracavity second-harmonic generation," Opt. Commun. **113**, 463 – 470 (1995).
37. T. Carmon and K. J. Vahala, "Visible continuous emission from a silica microphotonic device by third-harmonic generation," Nature Physics **3**, 430–435 (2007).
38. B. Corcoran, C. Monat, C. Grillet, D. Moss, B. Eggleton, T. White, L. O'Faolain, and T. Krauss, "Green light emission in silicon through slow-light enhanced third-harmonic generation in photonic-crystal waveguides," Nature photonics **3**, 206–210 (2009).
39. J. S. Levy, M. A. Foster, A. L. Gaeta, and M. Lipson, "Harmonic generation in silicon nitride ring resonators," Optics express **19**, 11415–11421 (2011).
40. O. Schubert, M. Hohenleutner, F. Langer, B. Urbanek, C. Lange, U. Huttner, D. Golde, T. Meier, M. Kira, S. Koch, and R. Huber, "Sub-cycle control of terahertz high-harmonic generation by dynamical bloch oscillations," Nature Photon. **8**, 119–123 (2014).
41. T. J. Kippenberg, R. Holzwarth, and S. Diddams, "Microresonator-based optical frequency combs," Science **332**,

555–559 (2011).
42. I. Ricciardi, S. Mosca, M. Parisi, P. Maddaloni, L. Santamaria, P. De Natale, and M. De Rosa, "Frequency comb generation in quadratic nonlinear media," Phys. Rev. A **91**, 063839 (2015).
43. F. Gravier and B. Boulanger, "Triple-photon generation: comparison between theory and experiment," J. Opt. Soc. Am. B **25**, 98–102 (2008).
44. S. Richard, K. Bencheikh, B. Boulanger, and J. A. Levenson, "Semiclassical model of triple photons generation in optical fibers," Opt. Lett. **36**, 3000–3002 (2011).
45. A. A. Kalachev and Y. Z. Fattakhova, "Generation of triphotons upon spontaneous parametric down-conversion in a resonator," IEEE J. Quant. Electron **37**, 1087–1090 (2007).
46. A. Hayat and M. Orenstein, "Photon conversion processes in dispersive microcavities: Quantum-field model," Phys. Rev. A **77**, 013830 (2008).
47. T. Felbinger, S. Schiller, and J. Mlynek, "Oscillation and generation of nonclassical states in three-photon down-conversion," Phys. Rev. Lett. **80**, 492 (1998).
48. C. Weedbrook, B. Perrett, K. V. Kheruntsyan, P. D. Drummond, R. C. Pooser, and O. Pfister, "Resonant cascaded down-conversion," Phys. Rev. A **85**, 033821 (2012).
49. K. S. Kunz and R. J. Luebbers, *The finite difference time domain method for electromagnetics* (CRC press, 1993).
50. J. D. Joannopoulos, S. G. Johnson, J. N. Winn, and R. D. Meade, *Photonic crystals: molding the flow of light* (Princeton Univ. Press, 2011).
51. H. Haus and W. Huang, "Coupled-mode theory," Proc. IEEE **79**, 1505–1518 (1991).
52. W. Suh, Z. Wang, and S. Fan, "Temporal coupled-mode theory and the presence of non-orthogonal modes in lossless multimode cavities," IEEE J. Sel. Topics Quantum Electron. **40**, 1511–1518 (2004).
53. R. Shugayev and P. Bermel, "Time-domain simulations of nonlinear interaction in microring resonators using finite-difference and coupled mode techniques," Opt. Express **22**, 19204–19218 (2014).
54. V. S. Ilchenko, A. B. Matsko, A. A. Savchenkov, and L. Maleki, "Low-threshold parametric nonlinear optics with quasi-phase-matched whispering-gallery modes," JOSA B **20**, 1304–1308 (2003).
55. M. Lakshmanan and S. Rajaseekar, *Nonlinear dynamics: integrability, chaos and patterns* (Springer Science & Business Media, 2003).
56. A. Hurwitz, "On the conditions under which an equation has only roots with negative real parts," Selected papers on mathematical trends in control theory **65**, 273–284 (1964).

1. Introduction

One of the key outstanding challenges associated with nonlinear optics since its inception [1] is obtaining strong interactions without exceeding the damage threshold for materials [2]. It has been theoretically predicted and experimentally confirmed that confining light in resonant cavities with high quality factors and small modal volumes can enhance light-matter interactions [3–18]. In addition, use of a cavity introduces phenomena not seen in bulk materials, such as resonant frequency shifts from self- and cross- phase modulation, limit cycle phenomena, bi- and multistability [3, 5, 6, 10, 11, 19–23]. Much theoretical and experimental work has focused on second order ($\chi^{(2)}$) nonlinear processes, such as second harmonic generation (SHG) [5, 8, 24–30], sum and difference frequency generation (SFG/DFG) [9, 31–34]), and optical parametric amplification (OPA) [35, 36]). For example, recent work has shown that the quantum limited frequency conversion can be achieved in a triply resonant $\chi^{(2)}$ cavity with a critical relationship between pump and idler power [32]. Based on these work, DFG in triply resonant cavities has been demonstrated to have potential applications in terahertz (THz) generation [10,11]. There has also been some recent theoretical work on third harmonic generation (THG) in a doubly-resonant Kerr cavity, which has already shown that 100% conversion efficiency can be achieved with critical input power [5]. The input power required to achieve high efficiency in this process is much lower than THG in singly resonant cavities or bulk nonlinear materials. A follow-up paper [6] analyzed the stability of solutions calculated in [5], which display interesting nonlinear dynamical behaviors, such as multistability and limit cycles. In addition, it has also analyzed the influence of self- and cross- phase modulation (SPM and XPM) on the number of stable steady-state solutions. Recent experimental work has also supported the principle that THG can be enhanced in microphotonic devices [37–39].

While the use of cavities is known to enhance nonlinear effects, every distinct nonlinear pro-

cess requires a new analysis. Although the author in [5] has shown the condition to achieve 100% efficiency in THG process, no one has theoretically studied a cascaded THG process in a triply resonant Kerr cavity ($\omega+\omega+\omega \rightarrow 3\omega$, $3\omega+3\omega+3\omega \rightarrow 9\omega$ as shown in Fig. 1(a). This cascaded process can be used to achieve higher order conversion. Compared to 9^{th} order harmonic generation, this process is much better understood, and requires much lower input power. Much like the standard THG process, cascaded THG processes will also show a limit cycle phenomenon. However, compared to a standard THG process, cascaded THG processes cannot achieve 100% conversion efficiency. In addition, the maximum theoretical efficiency may not be stable in operation. Therefore, cavity parameters (quality factor in each resonant mode, nonlinear integral overlap, self- and cross- phase modulation terms) should be designed with specific optimal ratios to approach 100% stable conversion, as discussed in detail in Sec. 3.1. Cascaded THG processes can be used to generate THz waves from microwave or THz sources, as in [40], but with dramatically lower input powers. On a related note, cascaded phenomena play a fundamental role in forming optical frequency combs in Kerr [41] and Pockels [42] media. Therefore, having a clear understanding of these cascaded processes will be helpful for the design of a optical frequency comb with high performance. Although only a two-step THG cascade is studied in detail here, the approach in this paper also applies to an n-step cascaded THG.

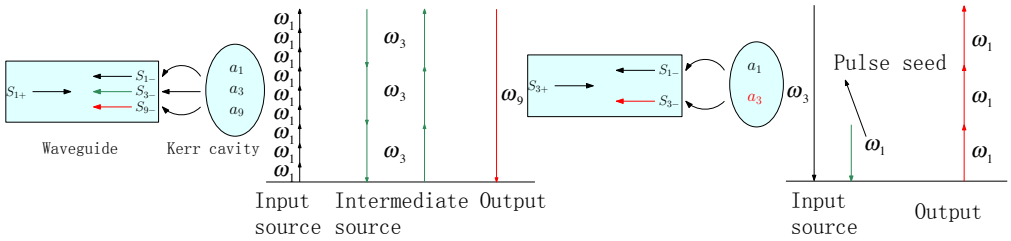

Fig. 1: (a) schematic for cascaded third harmonic generation (b) schematic for three-photon parametric down conversion involving a coupled waveguide-cavity system. The nonlinear system contains a waveguide used for input (output) photon flow coupled to a resonant cavity with multiple resonant modes. $|a_i|^2$ represents the number of photons in i_{th} mode, and $|S_{i+/-}|^2$ represents the number of input/output photons per second. In both figures, $\omega_1 = \omega, \omega_3 = 3\omega, \omega_9 = 9\omega$.

Another type of nonlinear phenomenon studied here is three photon parametric down conversion (3PDC) in a doubly resonant cavity ($3\omega \rightarrow \omega+\omega+\omega$, as shown in Fig. 1(b). Most studies focus on the down conversion in $\chi^{(2)}$ materials, and even do not even consider using $\chi^{(3)}$ materials because of their low efficiencies. Some of previous work has studied the three photon spontaneous parametric down conversion (SPDC) in $\chi^{(3)}$ optical bulk materials [43], fibers [44], resonators [45–48] by both semiclassical or quantum field theory. However, three-photon SPDC has a very high threshold power; thus the conversion efficiency is typically extremely low ($\sim 10^{-20}$ [44]). In this paper, we will study three photon parametric down conversion (3PDC) with a pulse at ω as a seed to excite high-efficiency conversion in a Kerr cavity, then analyze its dynamical process. This method can both dramatically lower the input power threshold while achieving up to 100% conversion efficiency at a critical input power, under ideal conditions, since it is not subject to the Manley-Rowe limits of DFG processes. In addition, the stabilities of all PDC processes will be analyzed in Sec. 3.2. This process has the potential to generate three entangled photons with high brightness for applications in quantum communi-

cation. This work will show that cascaded 3PDC cannot be achieved in a single, triply-resonant Kerr cavity, in contrast with cascaded THG. But we propose another method, which combines two doubly resonant Kerr cavities and three waveguides to achieve cascaded 3PDC, suitable for generating many low-energy photons, e.g., for THz communication.

This paper uses temporal coupled mode theory (TCMT) to analyze the cascaded THG and 3PDC process. In Sec. 2, we will first introduce the advantages of this method and derive equations for conversion efficiency calculation and stability analysis. Sec. 3 will be divided into three parts. In the first part (Sec. 3.1), we will show how to achieve high-efficiency stable nonlinear generation in cascaded THG process in the absence of SPM and XPM based on the theory in Sec. 2. In the second part (Sec. 3.2), conversion efficiency in 3PDC will be calculated and stability of steady-state solutions will be analyzed. In addition, we will demonstrate that cascaded 3PDC in a triply resonant Kerr cavity is impossible, and will propose an alternative method to achieve cascaded 3PDC. And in Sec. 3.3 , we briefly consider the effects of SPM and XPM by using a simple model to illustrate the qualitative behavior of the system; in particular, we demonstrate the existence of stable, maximal-efficiency solutions, including SPM and XPM effects.

2. Theory

2.1. Temporal coupled mode theory (TCMT)

TCMT is a fairly general method of studying optical mode interactions even for complex systems with nonlinearities, assuming each mode is well-defined. Several numerical methods can also be applied to simulate multi-mode nonlinear systems in the time domain. Among these, the FDTD (finite-difference time domain) [49] method which directly solves the Maxwell equations, is the most general and flexible method. However, this method is very time and memory consuming which makes exploration of multi-dimentional parameter spaces challenging. Instead, one can simplify the computation by focusing on the most critical degrees of freedom – the amplitude and phase of a small set of normal modes. It can be shown that optical problems coupling these modes can be analyzed using very general principles, such as the conservation of energy. The optical process in the system can be described by a universal set of ODEs in terms of several coefficients, which is determined by geometry and material of the system [50]. This approach is called temporal coupled mode theory (TCMT). It was first proposed by Haus *et al.* [51] and be expanded to a more general form by W. Suh *et al.* [52]. It has recently been shown that TCMT can accurately reproduce the nonlinear dynamics of complex nanophotonic systems simulated in the time-domain more than an order of magnitude faster [53] and was used to predict the threshold power of PDC in a spherical WGM resonator [54]. In this paper, we employ TCMT to characterize the behavior of intracavity cascaded THG and three photon PDC systems. Under the assumption of time-reversal invariance, we can derive the equations of the coupling between cavity modes and input/output source [50].

$$S_{i-} = -S_{i+} + \sqrt{2\gamma_i}a_i, \tag{1}$$

where $|a_i|^2$ represents the number of photons in mode i, $|S_{i+}|^2$ ($|S_{i-}|^2$) represents the number of photons per second goes into (out from) mode i.

The TCMT equations for a general nonlinear Kerr cavity are rigorously derived by first quan-

tization in the Heisenberg picture [53], which yields:

$$\begin{aligned}
\frac{da_1}{dt} =&[-\gamma_1 + i\omega_1^{cav}(1-\omega_1^2 m_{11}|a_1|^2 - \omega_1\omega_3 m_{13}|a_3|^2)]a_1 + \sqrt{2\gamma_{s,1}}S_{1+} - i3M_1\sqrt{\omega_1^3\omega_3}a_3(a_1^*)^2 \\
\frac{da_3}{dt} =&[-\gamma_3 + i\omega_3^{cav}(1-\omega_1\omega_3 m_{31}|a_1|^2 - \omega_3^2 m_{33}|a_3|^2 - \omega_3\omega_9 m_{39}|a_9|^2)]a_3 - iM_1^*\sqrt{\omega_1^3\omega_3}a_1^3 \\
&- i3M_2\sqrt{\omega_3^3\omega_9}a_9(a_3^*)^2 \\
\frac{da_9}{dt} =&[-\gamma_9 + i\omega_9^{cav}(1-\omega_3\omega_9 m_{93}|a_3|^2 - \omega_9^2 m_{99}|a_9|^2)]a_9 - iM_2^*\sqrt{\omega_3^3\omega_9}a_3^3
\end{aligned} \tag{2}$$

Here, γ_i means the decay rate of one specific resonant mode consisting of two components. $\gamma_{s,i}$ is the decay rate into S_{i-}, and $\gamma_{et,i}$ is the rate of external losses, so that $\gamma_i = \gamma_{s,i} + \gamma_{et,i}$. The a_i, S_i in Eq. (2) is different from the a_i, S_i in references [5, 6, 10, 50], where $|a_i|^2$ represents the energy in each resonant mode, $|S_i|^2$ represents the power of the input/output source, and ω_i^{cav} represents the resonant frequency of each mode. In this paper, since equations in Eq. (2) are derived by first quantization, $|a_i|^2$ represents the number of photons in resonant mode i and $|S_{i,+/-}|^2$ represents the input/output number of photons per second. Nonlinear coefficients m_{ij} and M_i are determined by the geometry and materials of the nonlinear system, and can reflect the strength of the nonlinear processes in this system. m_{ij} is called self- ($i = j$) or cross- ($i \neq j$) phase modulation term, which will shift the cavity resonant frequencies. Although detuning via dispersion and self- and cross-phase modulation is allowed in Eq. (2), much of our discussion assumes that pre-tuning is performed such that $\omega_i^{cav} = \omega_i$. This assumption leads to the best conversion efficiencies, and is still a reasonable assumption when $|\omega_i^{cav} - \omega_i| \ll \gamma_i$. M_i, which is also called nonlinear integral overlap, characterizes energy transfer ability between different modes. The expression for both m_{ij} and M_i terms are shown in Eq. (3).

$$\begin{aligned}
M_i &= \frac{\hbar^2}{8}\frac{\int dr\varepsilon_0\chi^{(3)}\left(E_{3^{i-1}}^*\right)^3 E_{3^i}}{\left[\int dr\varepsilon|E_{3^{i-1}}|^2\right]^{3/2}\left[\int dr\varepsilon|E_{3^i}|^2\right]^{1/2}} \\
m_{ij} &= \frac{3\hbar^2}{4*(1+\delta_{ij})}\frac{\int dr\varepsilon_0\chi^{(3)}\left|E_iE_j\right|^2}{\left[\int dr\varepsilon|E_i|^2\right]\left[\int dr\varepsilon\left|E_j\right|^2\right]}
\end{aligned} \tag{3}$$

where E_i represents the electrical field in specific resonant mode. From above equations, we can see that both $m_{i,j}$ and M_i terms scale with $1/V$, so the absolute values of these items are related to the modal volume. A detailed derivation of Eqs. (2) and (3) is given in Appendix A.

The equations describing 3PDC are very similar, except that the input source term is now changed from S_{1+} to S_{3+}:

$$\begin{aligned}
\frac{da_3}{dt} =&[-\gamma_3 + i\omega_3^{cav}(1-\omega_1\omega_3 m_{31}|a_1|^2 - \omega_3^2 m_{33}|a_3|^2)]a_3 - iM_1^*\sqrt{\omega_1^3\omega_3}a_1^3 + \sqrt{3\gamma_{s,3}}S_{3+} \\
\frac{da_1}{dt} =&[-\gamma_1 + i\omega_1^{cav}(1-\omega_1^2 m_{11}|a_1|^2 - \omega_1\omega_3 m_{13}|a_3|^2)]a_1 - i3M_1\sqrt{\omega_1^3\omega_3}a_3(a_1^*)^2
\end{aligned} \tag{4}$$

2.2. Conversion efficiency calculation and stability analysis method

In this section, we will first show how to calculate efficiency at steady-state, and then the stability of those calculated fixed points will be analyzed.

2.2.1. Efficiency calculation in TCMT

In TCMT, the set of resonant modes $a_i = \sqrt{r_i}e^{i\phi_i}e^{i\omega_i t}$, where ϕ_i represents the phase of this mode, and $\sqrt{r_i}$ represents the amplitude. At steady-state, both the amplitude $\sqrt{r_i}$ and phase

ϕ_i of a_i should be fixed, such that $dr_i/dt = 0$ and $d\phi_i/dt = 0$. The conversion efficiency of the cascaded THG process (i.e., the ratio between output power at 9ω and input power at ω) can be expressed as $\eta = 9\left|S_{9-}/S_{1+}\right|^2 = (18\gamma_9 r_9)/\left|S_{1+}\right|^2$. Here, r_9 can be obtained by requiring Eq. (2) to satisfy the stationary conditions for the amplitude and phase, and solving analytically. A similar calculation can be made to obtain the conversion efficiency for three photon down conversion ($\eta_{PDC} = \frac{1}{3}\left|S_{1-}/S_{3+}\right|^2$).

2.2.2. Stability analysis of fixed points

The commonly used method to analyze the stability of a steady state solution of nonlinear dynamical equations is to solve for the eigenvalues of the Jacobian matrices about the fixed point [55]. If the real part of each eigenvalues is negative, then the solution is stable. If we assume r_i^0, ϕ_i^0 to be the steady-state amplitude and phase under the driving source, the Jacobian matrices for the amplitude J_r and phase J_ϕ of the cascaded THG processes are given by:

$$J_r = \begin{bmatrix} -\left(\gamma_1 + 6\gamma_3 \frac{r_3^0}{r_1^0} + 18\gamma_9 \frac{r_9^0}{r_1^0}\right) & -(3\gamma_3 + 9\gamma_9 \frac{r_9^0}{r_3^0}) & 0 \\ 3\gamma_3 \frac{r_3^0}{r_1^0} + 9\gamma_9 \frac{r_9^0}{r_1^0} & -\gamma_3 - 6\gamma_9 \frac{r_9^0}{r_3^0} & -3\gamma_9 \\ 0 & 3\gamma_9 \frac{r_9^0}{r_3^0} & -\gamma_9 \end{bmatrix}, \; J_\phi = \begin{bmatrix} -\gamma_1 + 6\gamma_3 \frac{r_3^0}{r_1^0} + 18\gamma_9 \frac{r_9^0}{r_1^0} & -\left(3\gamma_3 \frac{r_3^0}{r_1^0} + 9\gamma_9 \frac{r_9^0}{r_1^0}\right) & 0 \\ 3\gamma_3 + 9\gamma_9 \frac{r_9^0}{r_3^0} & -\left(\gamma_3 + 2\gamma_9 \frac{r_9^0}{r_3^0}\right) & -3\gamma_9 \frac{r_9^0}{r_3^0} \\ 0 & 3\gamma_9 & -\gamma_9 \end{bmatrix} \quad (5)$$

The eigenvalues of above matrix can be analyzed by using the Routh-Hurwitz algorithm [32, 56]. The characteristic polynomial for the eigenvalues of Eq. (5) can be written in the form $\lambda^3 + B\lambda^2 + C\lambda^2 + D = 0$. Signs of the real parts of the Jacobian matrices' eigenvalues will all be negative if and only if $B > 0$, $D > 0$, and $BC - D > 0$. In cascaded THG, we conclude that the steady-state amplitudes are unconditionally stable, while phase stability will be determined by both cavity parameters (e.g., quality factors of each resonant mode and susceptibility of material) and input source. For three-photon PDC, the corresponding Jacobian matrices are very similar, but the opposite situation obtains: the phase terms are unconditionally stable, while the amplitude stability depends on cavity parameters and the input source.

3. Results and discussion

In this section, we consider cascaded THG processes (Subsection 3.1) as well as three-photon and cascaded three photon parametric down conversion processes (Subsections 3.2 and 3.3). In both cases, the steady-state solutions based on temporal coupled-mode theory are calculated, with their stability analyzed using the equations in Sec. 2.2. For convenience, the efficiency of $\chi^{(3)}$ nonlinear conversion processes in cavities will first be calculated in the absence of self- and cross-phase modulation terms in above sections, i.e., $m_{ij} = 0$ (Subsection 3.2). The influence of self- and cross- phase modulation terms will be analyzed in Subsection 3.3.

3.1. Cascaded THG

Without loss of generality, we can choose a set of specific parameters for one cavity (e.g., in this paper, $\gamma_0 = \gamma_1 = \gamma_3 = \gamma_9 = 10^{-4}$, $M_0 = M_1 = M_2 = 10^{-6}\,\hbar^2\chi^{(3)}/a$, where a is the lattice constant of a photonic crystal cavity [50]). The influence of varying these parameters on the conversion efficiency and stability will be discussed later. By applying these parameters to our prior conversion efficiency expression, we can plot it as a function of the input power, as shown in Fig. 2. At low input power, the conversion efficiency is stable, but after the power increases to the "Maximum stable efficiency point", the conversion in the cavity system becomes unstable, entering a limit cycle. In addition, the calculation tells us that the calculated efficiency peak is unstable, and the maximum stable efficiency is much lower than this peak. The average efficiency in the limit cycle region (purple solid line in Fig. 2) is much lower than the calculated efficiency. Unlike THG processes, where the maximum theoretical efficiency can reach

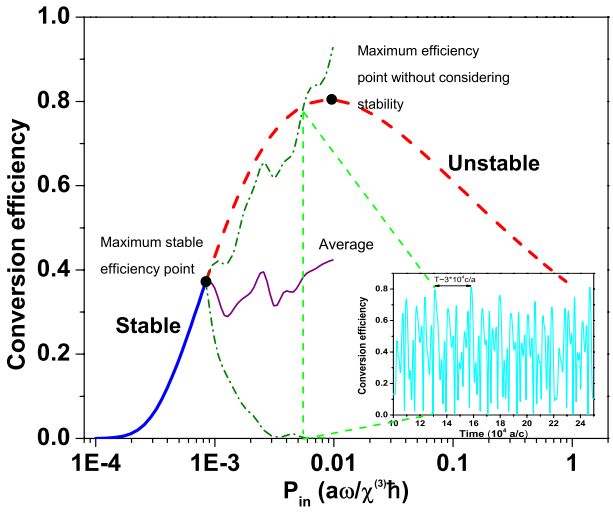

Fig. 2: Conversion efficiency in the function of input power. The blue solid line shows the stable conversion efficiency, and red dash line shows the unstable calculated efficiency in steady-state. The maximum stable efficiency (37%) is much lower than the maximum efficiency without considering stability (80%). In unstable region, the system goes into limit cycle and the efficiency fluctuates with time which is shown in inset. The dark green dash dot line shows the bounds of limit cycle in the unstable region from time domain simulation, where the solid purple line shows the average efficiency.

100% (neglecting extrinsic losses), complete frequency conversion cannot be achieved in cascaded THG processes. Therefore, we need to find an alternative method to approach the 100% efficiency.

3.1.1. Adjusting ratios of field overlap and decay rates

In the absence of self- and cross- phase modulation terms, five parameters determine the outcome of the nonlinear conversion process. In this section, we will explore the change of conversion efficiency by varying the ratio between two nonlinear integral overlap terms (M_1/M_2) and the ratio between decay rate of three resonant modes ($\gamma_1 : \gamma_3 : \gamma_9$). In Appx. B, we will demonstrate that the absolute value of system parameters (e.g., γ_i, M_i) will not affect the maximum stable conversion efficiency.

Figure 3 shows the conversion efficiency as a function of the field overlap ratio M_2/M_1 ($\gamma_1 : \gamma_3 : \gamma_9 = 1 : 1 : 1$ is fixed). If stability is ignored, the conversion efficiency will increase monotonically with M_2/M_1 near 1, since the output at 9ω mode will be enhanced, while the output at 1ω and 3ω will be suppressed. Thus, the result shown in the purple curve agrees well with the definition of M_1 and M_2. However, this picture changes in the presence of stability, as shown in the blue curve. Here, the actual maximum conversion efficiency does not increase monotonically with M_2/M_1, but shows a peak for M_2/M_1 near 1. This is because an exceedingly high M_2/M_1 will eliminate the balance between the two steps of the cascaded conversion process.

Next, we will explore the dependence of the maximum stable conversion efficiency on the

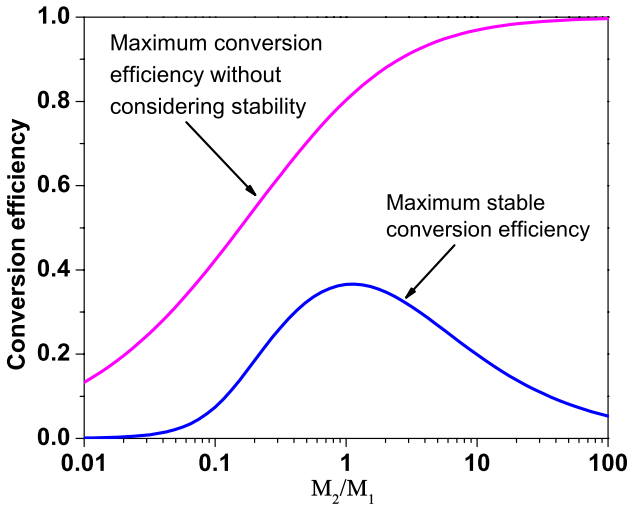

Fig. 3: Conversion efficiency versus field overlap ratio M_2/M_1 in two cases: the purple line ignores stability, while the blue line requires it. In the former, the maximum conversion efficiency increase monotonically with M_2/M_1. However, in the latter case, the maximum conversion efficiency peaks when M_2/M_1 near 1.

ratios of the decay rate of the three resonant modes; the procedure of varying all the decay rate ratios is shown in Fig. 4. One decay rate is varied at a time, while holding the other two constant, which divides the problem into three cases (change γ_1, change γ_3, and change γ_9). In addition, for each case, the problem has two conditions, e.g., if we change γ_1, γ_3 will either be bigger or smaller than γ_9. In order to obtain the highest maximum conversion efficiencies, the output at 9ω should be enhanced, while the output at 1ω and 3ω should be suppressed. From Eq. (1), the output at 3ω and 9ω is proportional to the decay rate and the energy stored in each mode. If γ_9/γ_3 is increased, the energy stored in 3ω will be increased, so the energy flow transferred from 3ω to 9ω will be increased ($da_9/dt \propto a_3^3$). As γ_9 increases, the energy stored in 9ω mode will be easier to output, so $|S_{9-}/S_{3-}|^2$ will be increased. Therefore, in order to obtain high conversion efficiency, γ_9 should be higher than γ_3 and γ_1. Furthermore, in order to obtain the highest conversion efficiency, γ_1 should also be higher than γ_3. This is because ω mode is the input mode, and its output can be expressed as $S_{1-} = -S_{1+} + \sqrt{2\gamma_1}a_1$, if γ_1 is too small, then a large part of input power will be reflected, which will lower the conversion efficiency. Therefore, in order to obtain the highest conversion efficiencies, the decay rates should satisfy the relation $\gamma_3 < \gamma_1 < \gamma_9$.

The results of exploring the six conditions summarized in Fig. 4 are shown in Fig 5. Subfigures (a) and (b) plot the maximum conversion efficiency as a function of γ_1/γ_0. From these two figures, the maximum conversion efficiency in the $\gamma_3 < \gamma_9$ condition is obviously higher than it in the $\gamma_3 > \gamma_9$ condition. In addition, we find that the maximum conversion efficiency plotted in Fig. 5(a) shows a peak as a function of γ_1/γ_0. Figure 5(c) and 5(d) plot the maximum conversion efficiency as a function of γ_3/γ_0. From Fig. 5(c) in which $\gamma_1 < \gamma_9$, we can see that the maximum conversion efficiency approaches 100% when γ_3 decreases. However, when $\gamma_1 > \gamma_9$, the result is the opposite. This is because although decreasing γ_3 can both enhance the

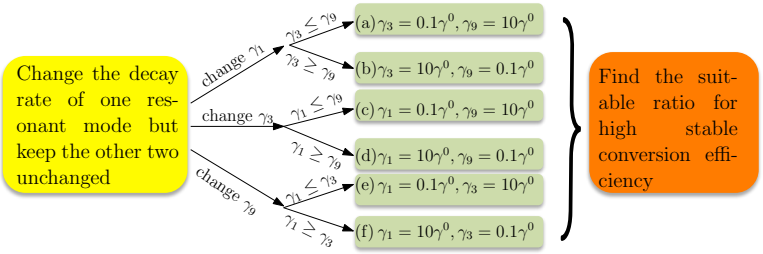

Fig. 4: The procedure for exploring all types of ratio between three resonant modes.

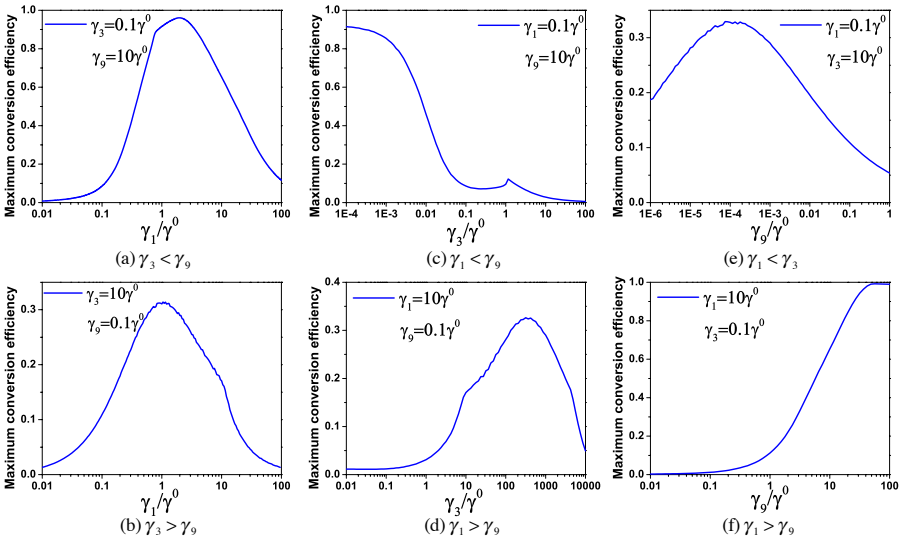

Fig. 5: The maximum conversion efficiency as a function of γ_i/γ_0. Following the procedure of Fig. 4, when γ_i is varied, the other two decay rates are fixed. In figure (a) and (b), γ_1/γ_0 is varied. In figure (c) and (d), γ_3/γ_0 is varied. In figure (e) and (f), γ_9/γ_0 is varied.

$P_{out,9}/P_{out,3}$ and $P_{out,1}/P_{out,3}$, in the case $\gamma_1 > \gamma_9$, the enhancement of the $P_{out,1}/P_{out,3}$ is larger than the enhancement of $P_{out,9}/P_{out,3}$. So the conversion efficiency drops with the decreasing of γ_3/γ_0. Figure 5(e) and 5(f) plot the maximum conversion efficiency as a function of γ_9/γ_0. The maximum conversion efficiency in the condition of $\gamma_1 < \gamma_3$ [Fig. 5(e)] is lower than it in the condition of $\gamma_1 > \gamma_3$ [Fig. 5(f)]. In addition, the maximum conversion efficiency increases with the increasing of γ_9/γ_0 in Fig. 5(f). Therefore, we can conclude that in order to approach 100% conversion efficiency, the decay rate of resonant mode should satisfy the condition $\gamma_3 < \gamma_1 < \gamma_9$, and the maximum conversion efficiency will increase monotonically with γ_9/γ_3 and γ_1/γ_3. We can extend this conclusion for the n^{th} cascaded THG process: to approach 100% conversion efficiency, the decay rate of the output mode should be largest, the decay rate of intermediate mode(s) should be smallest, and the decay rate of input mode should fall between those values.

As shown in Fig. 6, we can examine the combined effect on the maximum stable conversion efficiency of varying M_2/M_1 and γ_3/γ_0. As shown in the top right inset figure of Fig. 6, if $\gamma_1 : \gamma_3 : \gamma_9$ is fixed, the conversion efficiency curve will always peak at a finite M_2/M_1. However, for a fixed M_2/M_1 ratio, as shown in both the contour plot and the right bottom inset figure, the

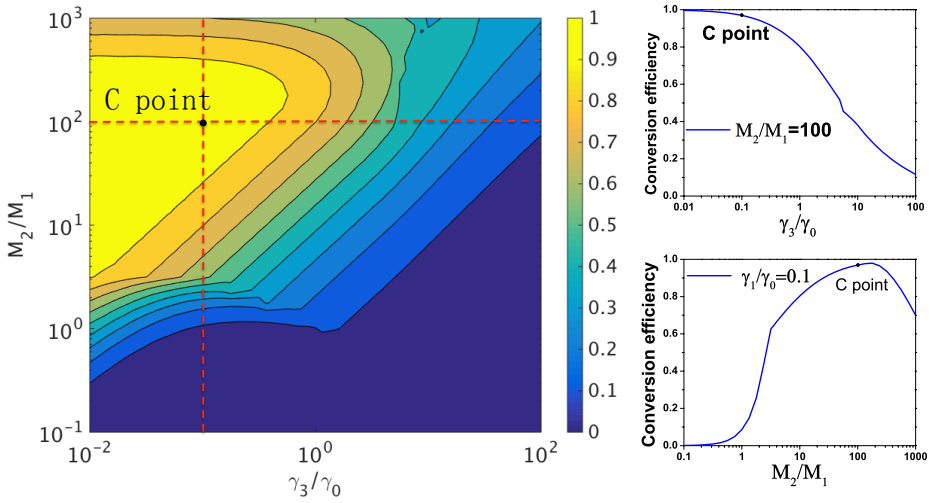

Fig. 6: Contour plot of maximum stable conversion efficiency as a function of M_2/M_1 and γ_3/γ_0. $\gamma_1 = 0.1\gamma_0$ and $\gamma_9 = 10\gamma_0$ are fixed. The right top inset figure shows the change of efficiency along the horizontal dash line. The right below inset figure shows the change of efficiency along the vertical dash line (M_2/M_1 is varied). C point in the figure represents the case where $\gamma_1 : \gamma_3 : \gamma_9 = 1 : 1 : 100$, $M_2/M_1 = 100$, and maximum stable conversion efficiency is 97%.

efficiency will always increase as γ_3 decreases, as predicted in the last paragraph.

3.2. Three-photon and cascaded three-photon parametric down conversion

Three-photon parametric down conversion (3PDC) is a nonlinear process that converts a photon at a frequency of 3ω to three photons at a frequency of 1ω; cascaded 3PDC extends this process n times in cases where sufficiently low frequencies cannot be achieved in a single step. If coherence is preserved, it can also generate three-photon entangled states.

3.2.1. Three-photon parametric down conversion

Similar to the procedure in Sec. 3.1, we will analyze 3PDC without considering phase modulation at first [e.g., $m_{ij} = 0$ in Eq. (4)). For convenience of plotting, the parameters in this section are set as $M_0 = M = 10^{-6}\hbar^2\chi^{(3)}/a$ and $\gamma_1 = 10^{-4}, \gamma_3 = 5\times10^{-4}$. Here, the γ_3 should be bigger than γ_1 as explained below.

As shown in Fig. 7, 3PDC efficiency as a function of input power peaks at 100% (neglecting extrinsic losses). In this condition, the complete depletion of the pump photons (ω) is required ($S_3 = 0$). If we set $P_{crit} = \hbar\omega_3 |S_{3+}|^2$, and apply $S_{3-} = -S_{3+} + \sqrt{2\gamma_3}a_3 = 0$, the critical power is given by:

$$P_{crit} = \hbar\omega_3 \left|S_{3+}^{crit}\right|^2 = \hbar\omega_3 \frac{2}{3M}\sqrt{\frac{\gamma_1^3\gamma_3}{3\omega_1^3\omega_3}}. \tag{6}$$

For input powers below a threshold P_T, parametric down conversion cannot occur, since the only solution has zero efficiency. Bifurcation into two solutions occurs above P_T: fortunately, the solution with higher conversion efficiency is stable, while the one with lower conversion efficiency is unstable. As mentioned before, the phase of steady-state solutions is stable, but amplitude is not automatically so. In order to make the amplitude of the steady-state stable, two

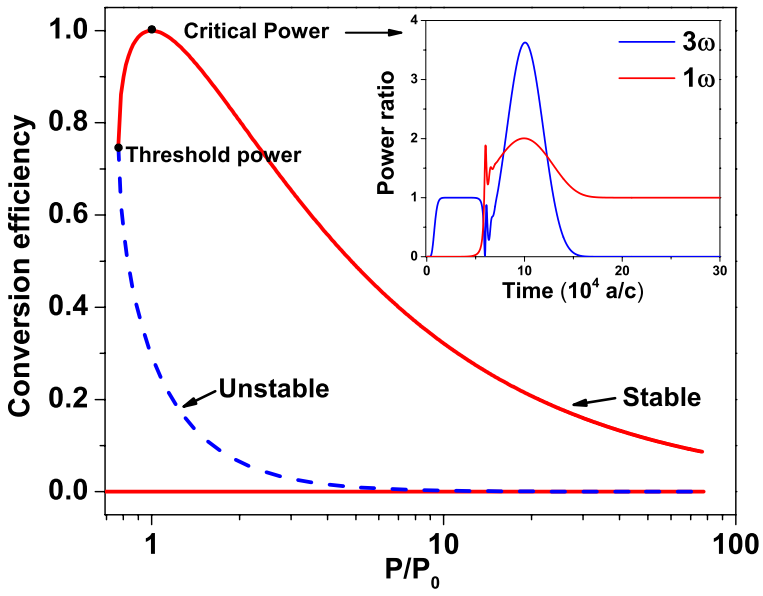

Fig. 7: Plot of the conversion efficiency from 3ω to 1ω as a function of P/P_0. Here, P is the input source power, and P_0 is the power of critical point as shown in the figure. The critical power is the power for 100% efficiency. The threshold power in the figure means the lowest power for PDC to start. In other words, if $P < P_T$, the conversion efficiency will always be zero. The inset shows time-dependent power ratios of the 1ω and 3ω modes at the critical power input for maximum conversion efficiency. The 3ω input source $S_{3+}(t) = S_{3+}^{crit}(1-e^{-t/\tau_1})e^{i3\omega t}$ gradually increases to a stable value, while the 1ω input $S_{1+} = S_{1+}e^{-(t-\tau_2)^2/\Delta t^2}e^{i\omega t}$ is a Gaussian pulse that seeds the conversion process.

conditions must be satisfied: (1) $\gamma_3 > \gamma_1$ and (2) $r_1/r_3 > \gamma_3/\gamma_1$. If the ratio r_1/r_3 is set to be $X = \gamma_3/\gamma_1$, we can use Eq. (4) to show that $S_{3+} = (X+3\gamma_1/\gamma_3)/\left[(\sqrt{2\gamma_3}/\kappa)(3\kappa/\gamma_1)^{3/2}X^{1/4}\right]$, where $\kappa = M\sqrt{\omega_1^3\omega_3}$. In order to calculate the threshold power for three photon PDC, we set the derivative of S_{3+} to zero, and obtain:

$$P_T = \hbar\omega_3\left|S_{3+}^{min}\right|^2 = \hbar\omega_3\frac{8}{27M}\sqrt{\frac{\gamma_1^3\gamma_3}{\omega_1^3\omega_3}} \approx 0.77P_{crit} \tag{7}$$

In addition, with power input P_T, the ratio of steady-state solution r_1 and r_3 is $r_1/r_3 = \gamma_3/\gamma_1$, which is equivalent to the stability condition. This explains why the threshold power point divides the bifurcation curve into two parts, where the higher efficiency is always stable and the lower efficiency is always unstable.

The inset figure of Fig. 7 shows the 3PDC power versus time. From the figure, we can see that the conversion efficiency is initially zero when the amplitude of the source with frequency of ω is very small. The oscillation between ω and 3ω starts when the amplitude of source with frequency of ω gradually increases. After the pulse the output power gradually stabilizes, for a time-averaged final conversion efficiency of 100%. Therefore, a 1ω "seed" pulse is necessary to catalyze 3PDC in cavities.

3.2.2. Cascaded three-photon parametric down conversion

As mentioned earlier, cascaded 3PDC in a triply resonant cavity is impossible. In this section, we will explain the reason by using the stability analysis method in Sec. 2. In the same fashion as in Section 2.2.2, the amplitude Jacobian matrix here can be calculated, and the Routh-Hurwitz algorithm can again be applied. However, we find two mutually contradictory conditions for B and $BC-D$; they should both be positive, yet we find if $B=\gamma_9-\gamma_1-\gamma_3$ is positive, then $BC-D=-\gamma_1\gamma_3(\gamma_1+\gamma_3)-\frac{5}{3}(\gamma_1+\gamma_3)\gamma_1^2 r_1/r_3-(-\gamma_1-\gamma_3+\gamma_9)\left[\gamma_1\gamma_9+\gamma_3\gamma_9+\frac{2}{3}\gamma_1\gamma_9 r_1/r_3+\frac{2}{3}\gamma_1\gamma_3 r_1/r_9+\frac{1}{9}\gamma_1^2 r_1^2/(r_3 r_9)+\gamma_3^2 r_3/r_9\right]-(\frac{2}{3}\gamma_1^2\gamma_3 r_1/r_9+\frac{1}{9}\gamma_1^3 r_1^2/r_3 r_9+\gamma_1\gamma_3^2 r_3/r_9)$ is always negative. This implies that cascaded photon down conversion cannot be achieved in a triply resonant Kerr cavity. Thus, we shall consider another method for multiple down conversion steps, which combines two doubly resonant cavity and three waveguides, as shown in Fig. 8.

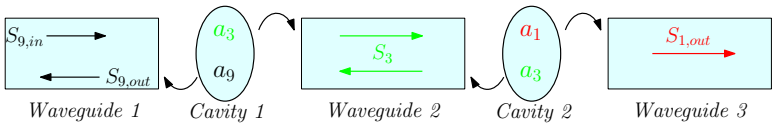

Fig. 8: Schematic for cascaded 3PDC involving a coupled waveguide-cavity system. The nonlinear system contains three waveguides. The left waveguide is used for input (output) source at 9ω. The middle waveguide used to transfer 3ω photons between cavities. And the right waveguide is used to output 1ω photons. The decay rate in cavity one are set as $\gamma_3^{cav(1)}$ and $\gamma_9^{cav(1)}$, and those in cavity two are set as γ_1^{cav2} and γ_3^{cav2}. Similarly, the nonlinear integral overlap in cavity one is $M^{cav(1)}$, and in cavity two is $M^{cav(2)}$.

If we set the decay rate in cavity 1 to γ_1 and γ_3, in cavity 2 to γ_3 and γ_9, then achieving 100% conversion efficiency requires equal input and output for the intermediate mode, or $\left|S_{3,out}^{cav(1)}\right|^2=\left|S_{3,in}^{cav(2)}\right|^2$. This is equivalent to the condition $\sqrt{[(\gamma_3^{cav(1)})^3\gamma_9^{cav(1)}/(\gamma_1^{cav(2)})^3\gamma_3^{cav(2)}]}=\frac{1}{3}M^{cav(1)}/M^{cav(2)}$, where $M^{cav(1)}$ and $M^{cav(2)}$ denotes the nonlinear field overlap integrals in cavity 1 and 2, respectively.

3.3. Self- and cross- phase modulation

3.3.1. Cascaded THG

In cascaded THG, nonlinear self- and cross-phase modulation could disrupt the conversion process by shifting the cavity frequencies. To offset this effect, we may pre-compensate the cavity frequencies based on the steady-state condition of Eq. (8):

$$\begin{aligned}\omega_1^{cav}&=\frac{\omega_1}{1-\omega_1\omega_3 m_{31}r_1^{crit}-\omega_3^2 m_{33}r_3^{crit}}\\ \omega_3^{cav}&=\frac{\omega_3}{1-\omega_1\omega_3 m_{31}r_1^{crit}-\omega_3^2 m_{33}r_3^{crit}-\omega_3\omega_9 m_{93}r_9^{crit}}\\ \omega_9^{cav}&=\frac{\omega_9}{1-\omega_3\omega_9 m_{93}r_3^{crit}-\omega_9^2 m_{99}r_9^{crit}}\end{aligned}\tag{8}$$

Here, we will explore the influence of self- and cross- phase modulation at the C point from Fig. 6. The r_i^{crit} represents the steady-state amplitude of a_i^2 – i.e., the number of photons required in the i_{th} resonant mode for maximum stable conversion efficiency. For convenience, we define: $m_{11}=m_{13}=m_{31}=\xi\times M_1$, $m_{93}=m_{39}=m_{99}=\zeta\times M_2$, $m_{33}=\sqrt{\xi\zeta}\times M_1M_2$.

The inclusion of self- and cross- phase modulation introduces new steady-state solutions (as shown in Fig. 9(a), but the original solution in the case $\xi = \zeta = 0$ still remains; the stabilities of the old and new solutions are then examined again using the method from Sec. 2.2.

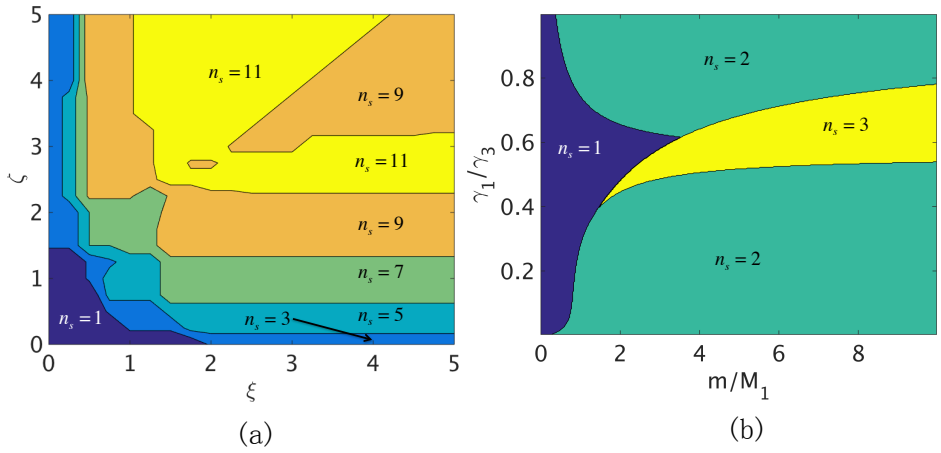

Fig. 9: (a) Contour plot of number of stable solutions n_s as a function of ξ and ζ , and the system parameters are based on point C in Fig. 6(b). Contour plot of number of stable solutions n_s (zero efficiency solution is not included) as a function of γ_3/γ_1 and m/M_1 for input power $P = P_T$.

3.3.2. Three photon PDC

For 3PDC processes, the inclusion of self- and cross- phase modulation will also shift the cavity resonant frequencies. Therefore, by using the same method mentioned in cascaded THG section, the resonant frequencies of cavity should be pre-compensated as in Eq. (8). The maximum stable conversion efficiency in 3PDC is always 100% and the analytical expression for critical input power can be derived. Compared to cascaded THG, where we can only analyze the influence of SPM and XPM for one specific set of cavity parameters (the C point in Fig. 6), we can perform a more general analysis of their influence on efficiency and stability for 3PDC.

The stability of the conversion is determined by γ_3/γ_1 and m_{ij}/M_1. If we define $\forall_{i,j} m \equiv m_{ij}$, this allows us to fully characterize variation in the number of stable steady-state solutions as a function of γ_3/γ_1 and m/M_1, as depicted in Fig. 9(b). This result is similar to the case of cascaded THG in Fig. 9(a). The inclusion of self- and cross- phase modulation introduces new steady-state solutions without destabilizing the original solution for $m_{ij} = 0$. One distinction is that instability in the steady-state solution for 3PDC may be caused by its amplitude, which differs from the potential phase instability of cascaded THG. Therefore, the nonlinear dynamical system of PDC will not follow a limit cycle, but will remain at one of the stable solutions.

For both cascaded THG and 3PDC, the inclusion of SPM and XPM will introduce multistable solutions. So it is necessary to find a method to excite the maximum-efficiency solution. The author in [6] has already proposed a simple method to excite the solution with maximum efficiency from several stable solutions in THG process. The cascaded THG process and 3PDC show more complex result compared to THG process, which may make it more difficult to excite high-efficiency solutions. How to excite the maximum-efficiency solution is beyond the scope of this paper, but in future we will study the method to excite highly efficient and stable solution in real Kerr cavity for both cascaded THG and 3PDC.

4. Conclusion

Using temporal coupled-mode theory, we have demonstrated two key results for frequency conversion of photons. First, we demonstrated that highly efficient and stable cascaded third harmonic generation (THG) can be achieved in a triply resonant cavity. Here, changing field overlap and cavity decay ratios proportionately will not change the maximum stable conversion efficiency; however, adjusting the ratios of these values with respect to one another yields a certain set of best values. Ideally, the decay rate of the intermediate frequency mode γ_3 should be small (i.e., the γ_9/γ_3 and γ_1/γ_3 ratios should be large). Second, we found the threshold power P_T at which three-photon parametric down conversion (3PDC) could be achieved for a doubly resonant cavity, as well as the critical power P_{crit} at which 100% conversion could be achieved with seeding (neglecting extrinsic losses, self- and cross-phase modulation). In addition, we demonstrated that cascaded 3PDC cannot be achieved directly in triply resonant Kerr cavities, but proposed an alternative using two doubly resonant Kerr cavities and three waveguides to achieve 100%-efficient cascaded 3PDC. The inclusion of SPM and XPM introduces more stable solutions with different conversion efficiencies, but the original solution in their absence still remains with unchanged stability. In a future manuscript, we plan to explore cascaded THG, 3PDC and cascaded 3PDC in realistic cavities such as nano beam cavities, ring resonators, or Fabry-Perot cavity, and study the method to excite the maximum-efficiency solution from multi-stable solutions.

Appendix A: Derivations for TCMT dynamic equations

In this section, we derive the TCMT equations for nonlinear frequency conversion in general Kerr nonlinear cavities. The electromagnetic field Hamiltonian in Kerr nonlinear media is:

$$H = \int dr\varepsilon_0 \left[\chi^{(1)}(r) + \chi^{(3)}(r)\left|E(r)\right|^2\right]\left[\varepsilon E(r)^2 + \frac{1}{\varepsilon\mu}B(r)^2\right] \tag{A1}$$

The electrical field can be expressed as $\hat{E}(r,t) = \sum_k C_k\left[\hat{a}_k g_k(r)e^{-i\omega_k t} + \hat{a}_k^\dagger g_k^*(r)e^{i\omega_k t}\right]$, where $\hat{a}_k$ and $\hat{a}_k^\dagger$ are the annihilation and creation operators, respectively. $g_k(r)$ represents the complete set of orthonormal modes.

In the absence of the Kerr effect, the electrical Hamiltonian is $H_{el,k} = C_k^2\int dr\varepsilon(r)\left|g_k(r)\right|^2(\hat{a}_k\hat{a}_k^\dagger + \hat{a}_k^\dagger\hat{a}_k)$. And after adding the magnetic energy part, the total Hamiltonian now becomes:

$$H_k = 2C_k^2\int dr\varepsilon(r)\left|g_k(r)\right|^2(\hat{a}_k\hat{a}_k^\dagger + \hat{a}_k^\dagger\hat{a}_k) \tag{A2}$$

In order for mode k to evolve with its characteristic frequency ω_k through the Heisenberg equation of motion, the equality $H = \frac{1}{2}\hbar\omega_k(\hat{a}_k\hat{a}_k^\dagger + \hat{a}_k^\dagger\hat{a}_k)$ must also hold. So the coefficient C_k can be expressed as:

$$C_k = \frac{1}{2}\sqrt{\frac{\hbar\omega_k}{\int dr\varepsilon(r)\left|g_k(r)\right|^2}} \tag{A3}$$

Now, taking nonlinearity into consideration, the Hamiltonian can be expressed as:

$$H = \sum_k \hbar\omega_k(\hat{a}_k^\dagger\hat{a}_k + \frac{1}{2}) + 2\sum_{i,j,k,l}\prod_{\phi=i,j,k,l} C_\phi \times \left[\hat{a}_\phi g_\phi(r)e^{-i\omega_\phi t} + \hat{a}_\phi^\dagger g_\phi^*(r)e^{i\omega_\phi t}\right] \tag{A4}$$

From the Heisenberg equation, the derivative of the annihilation operator is $\frac{d\hat{a}_i}{dt} = \frac{1}{i\hbar}[\hat{a}_i, H]$. The commutator relation between annihilation and creation operators is $\left[\hat{a}_i, \hat{a}_j^\dagger\right] = \delta_{ij},\ [\hat{a}_i, \hat{a}_j] = 0$.

If we assume that the reaction happens in a cavity with $\omega, 3\omega, 9\omega$ three resonant modes and $i = 1, \omega_1 = \omega$, then the evolution of a_1 can be expressed as:

$$\frac{d\hat{a}_1}{dt} = -i\omega_1\hat{a}_1 - \frac{2i}{\hbar}C_1\left[g_1^*(r)e^{i\omega t}\right]\sum_{j,k,l}\prod_{\phi=j,k,l}C_\phi \times \left[\hat{a}_\phi g_\phi(r)e^{-i\omega_\phi t} + \hat{a}_\phi^\dagger g_\phi^*(r)e^{i\omega_\phi t}\right] \tag{A5}$$

Here, $e^{i(\omega_i \pm \omega_j \pm \omega_k \pm \omega_l)t}$ should not vary with time, so that $\omega_i \pm \omega_j \pm \omega_k \pm \omega_l = 0$ should be satisfied. Since $\hat{a}_k^\dagger \hat{a}_k |\Psi\rangle = n|\Psi\rangle$ and n means number of photon in mode k, we can also write $\hat{a}_k$ as a_k, $\hat{a}_k^\dagger$ as a_k^*, and $|a_k|^2$ as number of photons. Then above equation can be written as:

$$\frac{da_1}{dt} = -i\omega_1(1 - \omega_1^2 m_{11}|a_1|^2 - \omega_1\omega_3 m_{13}|a_3|^2)a_1 - iM_1\sqrt{\omega_1^3\omega_3}a_3(a_1^*)^2, \tag{A6}$$

where m_{11} is the self-phase modulation term, representing the case where $\omega - \omega + \omega - \omega = 0$, which can be expressed as $m_{11} = 2 \times 3!/2! \times (C_1)^4/\omega_1^2$, m_{13} is the cross-phase modulation term, representing the case where $\omega - \omega + 3\omega - 3\omega = 0$, which can be expressed as $m_{13} = 2 \times 3! \times (C_1)^2(C_3)^2/(\omega_1\omega_3)$, and M_1 is the nonlinear integral overlap, representing the case where $\omega + \omega + \omega - 3\omega = 0$, which can be expressed as $M_1 = 2 \times 3!/2! \times (C_1)^3 C_3/[(\omega_1)^{3/2}(\omega_3)^{1/2}]$.

Finally, by applying the above analysis method to other two modes, and adding the cavity loss and input source terms into the equations, the TCMT equations for cascaded THG, Eqs. (2) and (3), can be fully derived.

Appendix B: Proportionate scaling of field overlap and decay rates

In this appendix, we will demonstrate that the absolute of system parameters will not affect maximum conversion efficiency. We consider the effects of proportionately scaling the nonlinear field overlap integral ($M_1 = M_2 \equiv \alpha M_0$), as well as the decay rate of each resonant mode. ($\gamma_1 = \gamma_3 = \gamma_9 \equiv \beta\gamma_0$). In brief, the power requirements vary with α and β, but the maximum conversion efficiencies remain unchanged.

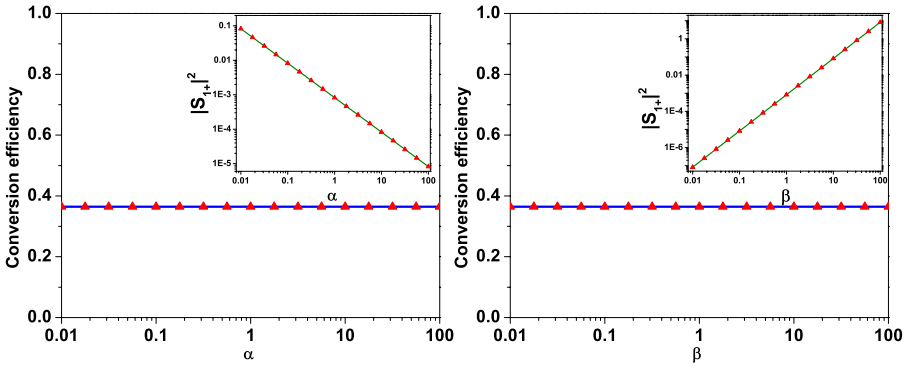

Fig. 10: (a) Maximum stable efficiency as a function of $\alpha \equiv M_1/M_0 = M_2/M_0$, as defined in Fig. 2. The inset shows the required input power for obtaining maximum stable efficiency. (b) Maximum stable efficiency as a function of $\beta \equiv \gamma_1/\gamma_0 = \gamma_3/\gamma_0 = \gamma_9/\gamma_0$. The inset shows the required input power for obtaining maximum stable efficiency.

Figure 10(a) shows that the maximum stable conversion efficiency is independent of $\alpha \equiv M_1/M_0 = M_2/M_0$, as defined in Fig. 2. The inset figure shows that the input power P_{in} required for maximum stable conversion efficiency is inversely proportional to α. The nonlinear integral overlap M_1 is proportional to the energy transfer rate from ω and 3ω, while M_2 corresponds to the energy transfer rate between 3ω and 9ω. Since energy transfer is enhanced by increasing both M_1 and M_2, the power required for achieving equal nonlinear conversion will be lowered (as shown in the inset figure of Fig. 10(a). At this newly lowered power, the final conversion efficiency remains unchanged.

Figure 10(b) shows that the maximum stable conversion efficiency is also independent of $\beta \equiv \gamma_1/\gamma_0 = \gamma_3/\gamma_0 = \gamma_9/\gamma_0$. The inset figure shows that the required input power for maximum stable conversion efficiency is proportional to β, since the stored energy in the cavity will decrease linearly with β for a constant input power. So the maximum stable conversion efficiency remains unchanged.

In summary, Fig. 10 demonstrates that the absolute value of system parameters (e.g. γ_i, M_i) will not affect the maximum stable conversion efficiency.

Acknowledgments

Support was provided by the Department of Energy, under DOE Cooperative Agreement No. DEEE0004946 (PVMI Bay Area PV Consortium), the Semiconductor Research Corporation, under Research Task No. 2110.006 (Network for Photovoltaic Technologies), and the National Science Foundation Award EEC 1454315 - CAREER: Thermophotonics for Efficient Harvesting of Waste Heat as Electricity.